

### 3B.3 A MODELING AND VERIFICATION STUDY OF SUMMER PRECIPITATION SYSTEMS USING NASA SURFACE INITIALIZATION DATASETS

Jonathan L. Case<sup>1\*</sup>, Sujay V. Kumar<sup>2</sup>, Jayanthi Srikishen<sup>3</sup>, and Gary J. Jedlovec<sup>4</sup>

<sup>1</sup>ENSCO Inc./Short-term Prediction Research and Transition (SPoRT) Center, Huntsville, AL

<sup>2</sup>SAIC/NASA Goddard Space Flight Center, Greenbelt, MD

<sup>3</sup>Universities Space Research Association (USRA), Huntsville, AL

<sup>4</sup>NASA Marshall Space Flight Center/SPoRT Center, Huntsville, AL

## 1. INTRODUCTION

One of the most challenging weather forecast problems in the southeastern U.S. is daily summertime pulse convection. During the summer, atmospheric flow and forcing are generally weak in this region; thus, convection typically initiates in response to local forcing along sea/lake breezes, and other discontinuities often related to horizontal gradients in surface heating rates. Numerical simulations of pulse convection usually have low skill, even in local predictions at high resolution, due to the inherent chaotic nature of these precipitation systems. Forecast errors can arise from assumptions within physics parameterizations, model resolution limitations, as well as uncertainties in both the initial state of the atmosphere and land surface variables such as soil moisture and temperature. For this study, it is hypothesized that high-resolution, consistent representations of surface properties such as soil moisture, soil temperature, and sea surface temperature (SST) are necessary to better simulate the interactions between the surface and atmosphere, and ultimately improve predictions of local circulations and summertime pulse convection.

The Short-term Prediction Research and Transition (SPoRT) Center has been conducting studies to examine the impacts of high-resolution land surface initialization data generated by offline simulations of the NASA Land Information System (LIS; Kumar et al. 2006, 2007) on subsequent numerical forecasts using the Weather Research and Forecasting (WRF) model (Case et al. 2008b). The NASA LIS is a high performance land surface modeling and data assimilation system that integrates satellite-derived datasets, ground-based observations and model reanalyses to force a variety of land surface models (LSMs). By using scalable, high-performance computing and data management technologies, LIS can run LSMs offline globally with a grid spacing as fine as 1 km to characterize land surface states and fluxes. Case et al. (2008b) presented improvements to simulated sea breezes and surface verification statistics over Florida by initializing the WRF model with land surface variables from an offline LIS spin-up run, conducted on the same WRF domain and resolution. In addition, Case et al. (2008c) demonstrated the ability to use both LIS land surface fields and high-resolution SSTs to initialize the surface and sub-surface variables

over a coastal domain, thereby providing a high-resolution lower boundary initial condition over the entire modeling domain.

The SPoRT Center has also developed high-resolution SST composites derived from the Moderate Resolution Imaging Spectroradiometer (MODIS) instruments aboard the NASA Aqua and Terra polar-orbiting satellites (Haines et al. 2007). The SPoRT Center has demonstrated the exquisite detail that can be depicted by these four-times-per-day composites compared to the once daily operational Real-Time Global (RTG) product used by the National Centers for Environmental Prediction (NCEP) models, which has a substantial impact on horizontal gradients in modeled sensible and latent heat fluxes over water bodies (LaCasse et al. 2008; Case et al. 2008a). They have also examined the sensitivity of WRF model simulations over oceanic regions to the high-resolution information, depicting the modifications to the nocturnal marine boundary layer under certain flow regimes over Florida. For example, LaCasse et al. (2008) depicted decreased static stability near the Florida East Coast under easterly flow regimes, and favored zones of low-level convergence near the coast under easterly flow and over the Gulf Stream under westerly flow. These model sensitivities to SSTs can have important implications to operations by providing modeled Planetary Boundary Layer (PBL) interactions with the detailed SSTs not currently available with any national or global product.

This current project extends the previous work done over Florida, now focusing on cases of typical pulse convection over the southeastern U.S., with an emphasis on improving the local short-term WRF simulations. This modeling study makes use of both the LIS land surface initialization and SPoRT MODIS SSTs to examine the sensitivity and possible improvements realized from these NASA capabilities. Furthermore, this study serves as a proof of concept to show that LIS and MODIS SST data can be easily incorporated into WRF for the benefit of organizations interested in running a local WRF application. The remainder of this paper is organized as follows. Section 2 describes the methodology for the current sensitivity experiment. Preliminary results are presented in Section 3, and a summary and vision for future work is given in Section 4.

## 2. EXPERIMENT DESIGN

A modeling sensitivity experiment is conducted with version 3.0.1.1 of the Advanced Research WRF (ARW; Skamarock et al. 2008) in which the land and

---

\*Corresponding author address: Jonathan Case, ENSCO, Inc., 320 Sparkman Dr., Room 3062, Huntsville, AL, 35805. Email: Jonathan.Case-1@nasa.gov

ocean/lake surface data from the NCEP North American Mesoscale (NAM) model is replaced with high-resolution data from a LIS offline simulation and MODIS SST composites, respectively. Details on the specific model configurations, initialization datasets, and verification methodologies are described below.

## 2.1 Model Configuration and Period of Study

This investigation consists of a set of Control and experimental ARW simulations initialized once per day at 0300 UTC from June to August 2008. The model is integrated 27 hours to 0600 UTC the following day, similar to some operational WRF runs done at NOAA/NWS Miami, FL and Mobile, AL. The simulation domain consists of a single grid of 309 x 311 staggered points in the zonal and meridional directions, respectively, at 4-km horizontal grid spacing, centered over the Southeastern United States. The grid contains 39 sigma-pressure vertical levels extending from the surface to a domain top of 50 mb. The vertical spacing is stretched from a minimum of 0.004 sigma near the surface (corresponding to ~40 m) to a maximum of 0.034 sigma at upper levels.

For both the Control and LIS+MODIS-initialized simulations (hereafter LISMOD), the ARW physics options consist of the rapid radiative transfer model (Mlawer et al. 1997) and the Dudhia scheme (Dudhia 1989) for longwave and shortwave radiation, respectively. The WRF Single Moment 6-class microphysics scheme (WSM6, Hong and Lim 2006; Skamarock et al. 2008) is used without any convective parameterization physics; thus, all convection is determined explicitly by the WSM6 microphysics and model dynamics. The planetary boundary layer and turbulence processes are parameterized by the Mellor-Yamada-Janjić scheme (Janjić 1990, 1996, 2002). Horizontal diffusion is handled by the two-dimensional Smagorinsky first-order closure scheme (Smagorinsky et al. 1965). All WRF runs use the Noah LSM as configured in version 3.0.1.1 of the ARW, being nearly identical to the version run operationally at NCEP (Chen and Dudhia 2001; Skamarock et al. 2008; Ek et al. 2003). Surface-layer calculations of friction velocities and exchange coefficients needed for the determination of sensible and latent fluxes in the LSM are provided by the NCEP Eta similarity theory scheme (Janjić 1996, 2002). The positive-definite advection options for moisture and scalars are enabled to remove the possible unphysical effects and high precipitation bias that can result from the “clipping” of negative mixing ratios in the 3rd order Runge-Kutta transport scheme (Skamarock and Weisman 2008; Skamarock et al. 2008).

For the Control runs, all initial conditions for the atmosphere, land, and RTG SSTs come from the native-resolution (12-km, grib 218) NCEP NAM model 3-h forecast initialized at 0000 UTC. Three-hourly boundary conditions for both the Control and LISMOD runs are provided by the NAM model 3-h to 30-h forecasts. The SSTs remain fixed throughout the 27-h ARW simulations. Interpolation of initial and boundary condition data are done with the WRF Pre-Processing System (WPS) utilities.

## 2.2 Initialization Data in Experimental Simulations

The LISMOD experimental runs are identical to the Control configuration except for the land surface initialization fields and the fixed SSTs. The land surface initial conditions of the Control are replaced by output from an offline LIS spin-up run. Meanwhile, the fixed RTG SSTs of the NAM model are replaced by the high-resolution SPoRT MODIS SST composites. Details on the LIS land surface and MODIS SST data, and how the data are incorporated into WRF are described in the sub-sections below.

### 2.2.1 LIS Initialization Data

For the offline LIS run, version 2.7.1 of the Noah LSM is run in LIS version 5 at the same horizontal resolution and center point as the WRF grid, but on a slightly larger domain to demonstrate that the WPS utilities can adequately interpolate the LIS data. Ideally, the LIS grid setup would be identical to the WRF simulation domain to avoid inconsistencies between the LIS and WRF soil fields introduced by horizontal interpolation. However, we aim to demonstrate a possible operational configuration in which SPoRT provides a generalized LIS initialization dataset to a variety of users (e.g. various NWS WFOs) running their own local WRF applications on domains that do not necessarily match the LIS grid. Such a scenario is probably the most practical method for providing LIS initialization data to multiple users.

For consistency, the Noah LSM in the offline LIS run uses the same soil and vegetation database as used by the WRF model. The soil type and properties are represented by the State Soil Geographic (STATSGO; Miller and White 1998) database. For the land-water mask and land cover, the U.S. Geological Survey 1-km global database derived from the Advanced Very High Resolution Radiometer (AVHRR) satellite data from 1992–1993 is up-scaled to the 4-km grid.

Additional required parameters used in the offline LIS runs include quarterly climatologies of albedo (Briegleb et al. 1986) and maximum snow-free albedo (Robinson and Kukla 1985), monthly climatologies of greenness fraction data derived from the AVHRR satellite (Gutman and Ignatov 1998), and a deep soil temperature climatology (serving as a lower boundary condition for the soil layers) at 3 meters below ground, derived from 6 years of Global Data Analysis System (GDAS) 3-hourly averaged 2-m air temperatures using the method described in Chen and Dudhia (2001).

The offline LIS run is cold-started on 1 January 2004 with a uniform first-guess soil temperature and moisture value. The Noah LSM is allowed to reach an equilibrium state during a spin-up integration of 4 years, 5 months from 1 January 2004 to 1 June 2008, using an integration time step of 30 minutes. Atmospheric forcings for the LIS run are provided by GDAS analyses (Derber et al. 1991). The GDAS has global coverage with three-hourly data at a horizontal resolution of 0.469° (~52 km). In addition, supplemental precipitation forcing from the Stage IV high-resolution analyses replaces the GDAS precipitation, providing much more detailed precipitation fields than GDAS. The Stage IV

product consists of hourly ~4-km precipitation analyses produced operationally by the U.S. River Forecast Centers, based on rain gauges and radar precipitation estimates from the Weather Surveillance Radar-1988 Doppler network (Lin and Mitchell 2005; Lin et al. 2005). The forcing fields are downscaled to the running resolution in LIS using bilinear or conservative (for precipitation) interpolation approaches. In the case of downward shortwave radiation, an additional zenith-angle based temporal disaggregation is applied. The forcing fields of downward-directed longwave radiation, pressure, 2-m air temperature and 2-m relative humidity are further topographically corrected via lapse-rate and hypsometric adjustments using the elevation data differences between the LIS grid and the native GDAS forcing grid.

The LIS is output in Gridded Binary-I format (GRIB1) daily at 0300 UTC for the period of record (June – August 2008) to initialize the WRF land surface fields in the LISMOD simulations. The GRIB1 formatted LIS data is used by the WPS with only a few minor modifications required. First, the output units in LIS soil moisture are changed to volumetric water content to be consistent with the units used in WPS/WRF. Second, the WPS file “METGRID.TBL” is modified to handle the LIS land-sea mask for interpolation of data to the WRF grid. The new LIS land-sea mask defined in METGRID.TBL is then applied to each of the land surface variables to be interpolated to the WRF grid. Finally, the interpolation method used in WPS for the LIS fields is a nearest-neighbor approach, as this method preserves the most detail and minimizes differences caused by interpolation. A summary of all the LIS fields incorporated into the WRF initial conditions is given in Table 1.

### 2.2.2 MODIS Sea Surface Temperatures

A 1-km MODIS SST composite, produced at the NASA SPoRT Center, is created by combining multiple passes of the Earth Observing System MODIS SST data (Haines et al. 2007). The compositing assumes that the day-to-day variation of SST is relatively small — the degree to which this assumption is valid will likely vary spatially and seasonally. Data from both the Terra and Aqua platforms are combined to create separate day/night composites. The composites examine the five most recent clear-sky SST values at each pixel. It then averages the warmest three of these five pixels in order to minimize the impact of cloud contamination.

Daytime (nighttime) passes through the composite region occur at approximately 1600 and 1900 UTC (0400 and 0700 UTC), respectively. The composites are output in GRIB1 format to ensure a seamless interpolation to the WRF grid with the WPS programs. Prior to being interpolated to the WRF grid, however, each 1-km MODIS SST composite is sub-sampled to a coarser grid with 2-km horizontal grid spacing due to limitations in array dimensions of the GRIB1 format.

Finally, the MODIS composite from 0400 UTC the previous day is incorporated into the daily WRF initial conditions at 0300 UTC to minimize diurnal variations in SST relative to the model initialization time. The only exception occurs for model initializations from 3–14 June 2008, when data are missing for the 0400 UTC

MODIS composites. For these LISMOD model initializations, the 0700 UTC MODIS composites from the previous day are used to initialize the SSTs.

## 2.3 Verification Methodology and Tools

For verifying precipitation and other fields in both the Control and LISMOD runs, the Meteorological Evaluation Tools (MET) package is employed. Created by the WRF Developmental Testbed Center at the National Center for Atmospheric Research, the MET package is a highly-configurable, state-of-the-art suite of model verification tools. It was developed using output from WRF but may be applied to the output of other modeling systems as well. MET provides a variety of verification techniques, including:

- Standard verification scores comparing gridded model data to point observations,
- Standard and neighborhood verification scores comparing gridded model data to gridded observations, and
- Object-based verification method comparing gridded model data to gridded observations.

More information on MET can be found at the web site <http://www.dtcenter.org/met/users/index.php>. An online User's Guide for MET version 2.0 is available at [http://www.dtcenter.org/met/users/docs/users\\_guide/MET\\_Users\\_Guide\\_v2.0\\_rev2.pdf](http://www.dtcenter.org/met/users/docs/users_guide/MET_Users_Guide_v2.0_rev2.pdf).

Our objectives for using MET at NASA/SPoRT is to incorporate a more standardized verification platform from which to conduct model evaluations. For this specific project, we are especially interested in capitalizing on the object-oriented verification methodology that has been implemented in MET. Known as the Method for Object-based Diagnostic Evaluation (MODE; Brown et al. 2007; Davis et al. 2009), this utility classifies “objects” in gridded fields, calculates a wide variety of object attributes, and merges/pairs forecast objects with observed objects to determine the similarities and differences between the various objects. We apply this utility to obtain more meaningful precipitation verification statistics for high-resolution forecasts of the pulse-type convection over the southeastern U.S.

## 3. PRELIMINARY RESULTS

This section provides preliminary results that illustrate some of the differences between the LIS land surface and MODIS SST initialization versus the interpolated NAM data in the Control runs. Sample forecast impacts are presented, as well as output from the MODE analysis tool available in the MET verification package.

### 3.1 Differences in Surface Initialization Datasets

The combination of LIS spin-up data and MODIS SSTs provides a considerably more detailed representation of the land and water surface compared to the Control run using interpolated 12-km NAM data. The depiction of 0–10 cm soil moisture at 0300 UTC 10 June 2008 in Figure 1 helps to illustrate this point. While the regional patterns of soil moisture are fairly similar, the LISMOD initialization data provides

information more consistent with the resolution of the WRF model in Figure 1b.

The difference field also indicates systematically drier initial conditions in this soil layer from southern Mississippi to northwestern South Carolina (Figure 1c). Over Florida, drier soil moisture is interspersed with local pockets of wetter soil moisture. These soil moisture variations are likely attributed to differences between the 12-km NAM Data Assimilation System (NDAS), which front-ends the NAM model, and the GDAS, which forces the LIS off-line run in combination with the Stage-IV precipitation analyses. Also, the ability of the 4-km LIS to better capture local areas of convective-type precipitation compared to the 12-km NDAS explains the local variations in soil moisture over Florida. It should be noted that the NDAS also uses the Stage-IV precipitation product to initialize its soil fields, similar to our offline LIS run.

A validation of the LIS versus Control (NAM) soil moisture was conducted at available observation sites from the U.S. Department of Agriculture's Soil Climate Analysis Network (SCAN, Schaefer et al. 2007). Several SCAN locations fall within the WRF modeling domain, but most sites are clustered in northern Alabama and western Mississippi (Figure 2a). Also worth noting is that all three SCAN sites in Florida were unavailable during the period of record. SCAN observes the soil temperature and volumetric soil moisture at depths ranging from 2 inches (5 cm) to 40 inches (102 cm) at most locations.

For validation purposes in the model, all observations made at levels lying within the model soil layers (0–10, 10–40, 40–100, and 100–200 cm) were compared to the model layer value at each daily 0300 UTC model initialization time. In some instances, the differences were computed using the same observation level for multiple layers. For example, the SCAN observations at 10 cm were used to validate the model values in both the 0–10 cm and 10–40 cm layers. Since the observations are measured at a single level while the modeled soil moisture is valid over a layer, the validation has representativeness issues and can be considered an "apples versus oranges" comparison. However, validation of soil moisture is quite hard to come by, and the SCAN observations are the best source of observed soil moisture data available in the experimental domain.

The results indicate that the LIS soil moisture was consistently drier in all layers relative to the NAM/Control soil moisture (Figure 2b). Based on the mean differences ("biases"), the NAM was slightly too moist relative to observations in the 0–10 cm layer while both the NAM and LIS were too dry in the three deepest layers. In all soil layers, the LIS mean differences were drier than the NAM, resulting in an increase of the dry bias in the 10–40, 40–100, and 100–200 cm layers relative to the observations. The 0–10 cm layer was the only layer in which the LIS mean difference was improved over the NAM. The root mean square (RMS) differences show that the LIS reduces the RMS difference/error in the top two layers, while increasing the RMS difference in the bottom two layers compared to the NAM (Figure 2b).

The mixed results make it difficult to determine which soil moisture initial field is consistently more accurate, especially considering the representativeness concerns between model layers and observed levels, as well as the sparseness and variable density of the SCAN observations. Much of the modeling domain does not have observations for validation. The main points we can conclude are that the LIS produced a drier overall soil layer compared to the NAM (at least at the SCAN locations), and that the 4-km LIS provides greater horizontal detail compared to the 12-km NAM fields.

The mean layer soil temperatures were also validated against the SCAN observations; however, the representativeness issue played an even larger role, resulting in a diurnal signal of the soil temperature differences when computed as a function of forecast hour. Consequently, soil temperature verification is not presented in this paper.

Meanwhile over the adjacent waters, the SPoRT MODIS SST product provides much more detail over the Gulf of Mexico and Atlantic waters compared to the interpolated RTG SSTs from the NAM model (Figure 3). For the model run initialized at 0300 UTC 10 June, SSTs were obtained from the 0700 UTC 9 June SPoRT/MODIS composite. Substantial differences (up to 2°C) are found in the vicinity of the shallow near-coastal waters near the Florida coast. For this particular composite, the MODIS tends to be cooler than the RTG.

The most noteworthy aspect of the MODIS composite is its ability to capture the fine-scale horizontal gradients in SSTs compared to the once-daily RTG product. The smoothness of the RTG data in Figure 3a precludes the model from capturing the relatively cool shelf waters off the Florida East Coast. However, the LISMOD SSTs in Figure 3b are able to depict the cool shelf waters and the magnitude of the Gulf Stream east of Florida. The SST differences illustrate the locally sharper horizontal gradients captured by the SPoRT MODIS product in Figure 3c.

### *3.2 Sample Forecast Sensitivities of Precipitation*

At first glance, the precipitation forecast sensitivities appear somewhat subtle, despite relatively significant changes in the details of the land and water initial conditions. A qualitative examination of several different days during the period of record (not shown) indicates that the broad patterns of forecast precipitation in the Control and LISMOD runs are generally similar, especially at longer accumulation intervals. Most of the differences in forecast precipitation arise from small-scale fluctuations in individual convective elements that evolve differently due to the variations in the land/water surface interactions with the PBL. If the Control forecast is significantly in error with the large-scale precipitation features, then the LISMOD is also generally in error. Therefore, it appears that the forecast precipitation in this model configuration is still largely driven by the atmospheric initial and boundary conditions, in addition to model dynamics and physics.

A sample 1-h forecast precipitation comparison ending 2100 UTC 10 June 2008 is presented in Figure 4. The flow pattern was very weak on this day, with no discernable boundaries or organized flow pattern over the southeastern U.S. Figure 4 shows how the forecast 1-h precipitation patterns and modes are quite similar overall in the Control and LISMOD runs. However, the difference field depicts numerous small-scale fluctuations between the forecasts (Figure 4c). Compared to the Stage-IV product in Figure 4d, both simulations over-predict precipitation across portions of Georgia and Mississippi, while under-predicting stratiform-type rainfall over northern Florida. So, it appears that the high-resolution input from LIS and MODIS SSTs led to numerous small-scale variations in the convective precipitation pattern, while the overall pattern of simulated precipitation remained nearly the same.

### 3.3 Selected Traditional Verification Statistics

Traditional point verification statistics at approximately 500 primary, mesonet, and cooperative stations over the southeastern U.S. were calculated using the MET package. The bias and RMS errors as a function of forecast hour (Figure 5a and b, respectively) for 2-m temperature and dew point temperature reveal relatively minor differences in most forecast hours. The bias plots (Figure 5a) indicate that the LISMOD develops a slightly higher warm bias by a few tenths of a degree Celsius between forecast hours 9 and 18, while a nominal dry dew point bias  $\leq 0.5^{\circ}\text{C}$  occurs between forecast hours 9 and 27. The total error represented by the RMS error in Figure 5b shows only very small differences between Control and LISMOD, with the LISMOD having marginally larger errors.

Using traditional grid-point by grid-point techniques, the 1-hour accumulated precipitation errors were also calculated using MET tools during the forecast hours of typical peak convective activity (12–24 hours, corresponding to 1500–0300 UTC). The results indicate that both the Control and LISMOD over-predict the area coverage of 1-hour accumulated precipitation at all 3 thresholds examined (bias  $> 1$  for 5-, 10-, and 25-mm per hour; Figure 6a). However, the LISMOD tends to reduce the bias between forecast hours 12–18, especially at the higher intensities. The Heidke Skill Score (HSS) in Figure 6b depicts a low skill under 0.10 for all precipitation thresholds that diminishes with forecast hour. The LISMOD has a marginally higher skill, mainly between forecast hours 12 and 18. Overall, the traditional error differences are quite minor and do not reveal any obvious performance differences in model accuracy, except for a reduction in the high-intensity precipitation bias.

### 3.4 MODE Object-Based Verification

The remainder of the analysis focuses on the non-traditional object-based verification available from MET's MODE tool. We first present a snapshot of forecast/observed object pairs from the Control and LISMOD simulation from 10 June, followed by overall composite results from running MODE over all 81 Control and LISMOD forecasts from summer 2008.

The object-matching in MODE is centered on an "interest function", which combines several attributes about the feature of interest — in this case 1-h accumulated precipitation from the WRF model (forecast) and Stage IV precipitation analyses (observed). The attributes consist of object characteristics such as centroid distance, minimum boundary distance, orientation angle difference, etc. MODE resolves objects in a gridded field through convolution thresholding. This technique involves applying a filter function to the raw data using a tunable radius of influence. The filtered field is then thresholded using another tunable parameter (typically the precipitation threshold) to create a mask field. Finally, the raw data are restored to objects where the mask meets/exceeds the specified threshold. More information on the technical details of MODE can be gleaned from Brown et al. (2007), Davis et al. (2009), and the MET User's Guide.

Forecast and observed objects are matched based on additional input criteria and a minimum value of the "interest function", which scales between 0 and 1. Our analysis focuses on 10 mm  $(1\text{ h})^{-1}$  precipitation objects during the peak convective forecast hours (12–24 h). The fuzzy engine weights used to formulate the interest function in our case are given in Table 2. Forecast/observed objects are considered matches if the interest function is  $\geq 0.6$  and the distance between the object centroids is no greater than 80 km. The interest function is not calculated for object pairs whose centroids are greater than 80 km apart.

#### 3.4.1 Output from 10 June 2008

Output from MODE for precipitation objects of 10 mm or greater for the 1-h period ending 2100 UTC 10 June is given in Figure 7. A comparison between the Control forecast and observed objects (Figure 7a, left column) shows about 4 small matched precipitation objects across the northern half of the Florida peninsula with several false alarm objects across southwestern Georgia, southeastern Alabama, and portions of south Florida. The LISMOD run has a similar pattern of 10-mm matched objects in northern Florida; however, there is a noticeable reduction in the false alarm objects over Georgia and Alabama.

It should be noted that if we had increased the object centroid distance criterion, modified the fuzzy weights in Table 2, and/or relaxed the interest function minimum threshold, then many more forecast and observed objects would have been matched together. For example, both the Control and LISMOD predicts 10-mm rainfall objects over the southeastern Florida coast in the vicinity of the observed precipitation areas, but the distances are too far to be considered matches. We used such a stringent requirement in order to minimize object matching for rainfall areas that a forecaster would not consider a "hit" (e.g. rainfall on the west coast of Florida being matched with objects on the east coast). Despite the somewhat stringent constraints placed on MODE, this configuration appeared optimal based on the level of detail and accuracy desired for this experiment.

Once the object matching is done, the total area of matched and unmatched objects is provided at each

forecast hour in the MODE output. A summary of the matched/unmatched objects areas (with forecast and observed objects combined together) indicates that the LISMOD out-performed the Control run on this day at many of the forecast hours (Table 3). Nine of the 13 hourly forecast periods have reductions in the unmatched areas in LISMOD, while 6 forecast hours have increases in the total matched area. Meanwhile, the Control experiences only 2 hourly forecasts with improvements in the matched/unmatched area over the LISMOD.

### 3.4.2 MODE Verification for Summer 2008

By applying the same object matching criteria to all 81 forecasts for the summer 2008, we can determine whether the LISMOD consistently out-performed the Control in 1-h precipitation forecasting accuracy during the peak convective hours. The matched and unmatched area for precipitation objects during the peak convective hours were summed for each Control and LISMOD forecast run. The difference between the total (un-)matched  $10 \text{ mm (1 h)}^{-1}$  precipitation areas in each forecast is plotted in Figure 8. Improvement in the LISMOD forecast is represented by positive blue bars (increase in matched area) and negative red bars (decrease in unmatched area). The LISMOD individual forecasts experience a wide range of improvement and degradation from run to run, so it is difficult to discern visually which model configuration consistently outperformed the other. However, there is a tendency for the LISMOD to have the largest increases in matched area (e.g. mid-August) and more numerous decreases in unmatched areas.

A summary of the mean matched/unmatched precipitation object areas per forecast run is provided in Table 4 for each of the three accumulated precipitation thresholds examined (5, 10, and 25 mm per hour). The LISMOD produces on average more matched and fewer unmatched object areas compared to the Control for all three thresholds between forecast hours 12–24. The lone exception is the matched area for  $25 \text{ mm (1 h)}^{-1}$ , in which the matched area averages the same in both the Control and LISMOD. All of the improvements in unmatched area were statistically significant at the 99<sup>th</sup> percentile, whereas only the 4.3% improvement in  $10 \text{ mm (1 h)}^{-1}$  matched area was marginally significant at the 90<sup>th</sup> percentile. All other changes to the matched area at other thresholds were non-significant.

The improvements to the forecast precipitation are also prevalent as a function of forecast hour, at least in the  $10 \text{ mm (1 h)}^{-1}$  threshold (Figure 9). During the peak convective times, the LISMOD consistently produced a slight increase in the matched area and a slight decrease in the unmatched area as a function of forecast hour (Figure 9a). The percentage change in matched/unmatched area indicates the greatest improvement earlier in the day between forecast hours 12 and 19 (Figure 9b). It should be noted that the  $5\text{-mm (1 h)}^{-1}$  also shows a notable improvement in the LISMOD, mainly from a reduction in unmatched area (not shown). However, the  $25\text{-mm (1 h)}^{-1}$  threshold did not show much of a clear distinction between the Control and LISMOD as a function of forecast hour.

Figure 10 provides a summary of the overall distribution of interest function values between forecast and object pairs at all forecast hours between 1500–0300 UTC for all 81 forecast days. Higher interest function values indicate that the forecast objects tend to be more similar in attributes to the corresponding observed objects. Among the three precipitation thresholds presented in Figure 10, the LISMOD has a larger interest value at higher percentiles in the distribution, particularly for the more intense precipitation thresholds. The LISMOD has a consistently higher interest value nearly everywhere in the distribution for the 25-mm threshold, and from the 50th to 90th percentiles for 10-mm threshold. The 5-mm interest values show little overall difference between Control and LISMOD. This result suggests that the LISMOD forecasts produced 1-hour accumulated precipitation areas that more closely resemble the observed rainfall areas, especially for more intense thresholds.

Finally, the accumulated precipitation in 3-hourly intervals was also examined using MODE, but did not show any distinctive signal between the Control and LISMOD (not shown). It could be that convective rainfall accumulation over a longer time period is difficult to discern into meaningful objects when the individual convective elements are chaotic in terms of the development and evolution.

## 4. SUMMARY AND FUTURE WORK

This paper describes a sensitivity experiment in which the interpolated land and ocean surface fields from the NCEP NAM model in a Control WRF model simulation are replaced with high-resolution datasets provided by unique NASA assets in an experimental simulation: the LIS and SPoRT/MODIS SSTs. The LIS is run in an offline mode for several years at the same grid resolution as the WRF model in order to provide WRF with compatible land surface initial conditions in an equilibrium state. The MODIS SSTs provide more detailed analyses of the SSTs over the oceans and large lakes compared to the RTG product used in the Control model runs.

Preliminary results indicate the LISMOD initial conditions contain much more detail, consistent with the WRF model resolution (as expected), when compared to the Control initial conditions. The large-scale patterns of soil moisture are fairly similar, but the LISMOD initial conditions do have some systematic regional differences, probably due to the LIS better resolving the fine-scale precipitation features of the Stage IV data compared to the 12-km NDAS. The MODIS SSTs are able to better capture the spatial variability in SSTs, especially in the waters surrounding the Florida peninsula. The forecast precipitation fields are fairly similar, especially in the overall larger-scale patterns; however, numerous small-scale differences occur.

Traditional verification methods do not reveal substantial differences between the two forecast configurations. Only slight differences in the 2-m temperature and dew point temperature errors are evident. The traditional grid point precipitation

verification does show a small reduction in the over-prediction of rainfall areas in LISMOD; however, the skill is almost equally as low in both experiments. Output from MODE's object-based verification within the MET package reveals that the LISMOD consistently generated precipitation objects that better matched observed precipitation objects, especially at higher precipitation intensities. The LISMOD runs also produced on average a 4% increase in matched precipitation areas and a simultaneous 4% decrease in unmatched areas (i.e. combination of false alarm and forecast misses).

Future efforts will include verifying the LIS soil moisture and temperature fields at Soil Climate Analysis Network sites over the southeastern U.S. In addition, we plan to examine the impacts of assimilating remotely-sensed and/or in situ soil moisture data, and introducing bi-weekly MODIS greenness vegetation fraction composites (as opposed to monthly climatologies) into offline NASA LIS runs and WRF simulations. Finally, the offline LIS runs could be transitioned into an operational mode similar to the MODIS SST composites, by providing high-resolution land surface fields and initialization data to NWS forecast offices in near real time.

## 5. ACKNOWLEDGEMENTS/DISCLAIMER

This research was funded by Dr. Tsengdar Lee of the NASA Science Mission Directorate's Earth Science Division in support of the SPoRT program at the NASA MSFC. Computational resources for this work were provided by the NASA Center for Computational Sciences at the NASA Goddard Space Flight Center. The lead author is also indebted to the invaluable assistance provided by John Halley-Gotway and others on the MET development team at NCAR.

Mention of a copyrighted, trademarked or proprietary product, service, or document does not constitute endorsement thereof by the authors, ENSCO Inc., SAIC, USRA, the SPoRT Center, the National Aeronautics and Space Administration, or the United States Government. Any such mention is solely for the purpose of fully informing the reader of the resources used to conduct the work reported herein.

## 6. REFERENCES

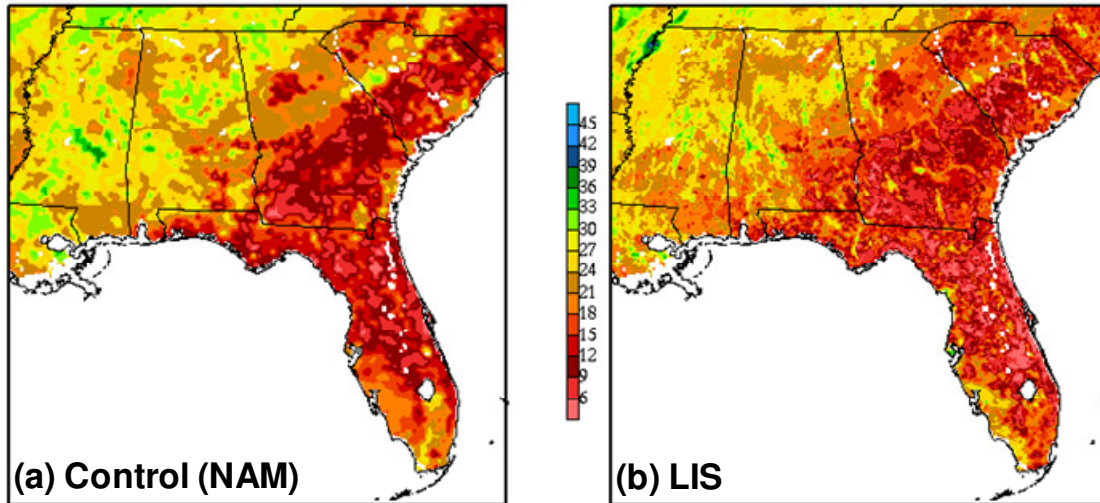
- Briegleb, B. P., P. Minnis, V. Ramanathan, and E. Harrison, 1986: Comparison of regional clear-sky albedos inferred from satellite observations and model computations. *J. Climate Appl. Meteor.*, **25**, 214-226.
- Brown, B. G., R. Bullock, J. Halley Gotway, D. Ahijevych, C. Davis, E. Gilleland, and L. Holland, 2007: Application of the MODE object-based verification tool for the evaluation of model precipitation fields. Preprints, *22nd Conf. on Weather Analysis and Forecasting and 18th Conf. on Numerical Weather Prediction*, Park City, Utah, Amer. Meteor. Soc., 10A.2. [Available online at <http://ams.confex.com/ams/pdfpapers/124856.pdf>]
- Case, J. L., P. Santos, M. E. Splitt, S. M. Lazarus, K. K. Fuell, S. L. Haines, S. R. Dembek, and W. M. Lapenta, 2008a: A multi-season study of the effects of MODIS sea-surface temperatures on operational WRF forecasts at NWS Miami, FL. Preprints, *12th Conf. on Integrated Observing and Assimilation Systems for Atmosphere, Oceans, and Land Surface*, New Orleans, LA, Amer. Meteor. Soc., 14.1. [Available online at <http://ams.confex.com/ams/pdfpapers/131892.pdf>]
- Case, J. L., W. L. Crosson, S. V. Kumar, W. M. Lapenta, and C. D. Peters-Lidard, 2008b: Impacts of High-Resolution Land Surface Initialization on Regional Sensible Weather Forecasts from the WRF Model. *J. Hydrometeor.*, **9**, 1249-1266.
- Case, J. L., G. T. Stano, M. E. Splitt, S. M. Lazarus, W. L. Crosson, W. M. Lapenta, G. J. Jedlovec, and C. D. Peters-Lidard, 2008c: High-resolution specification of the land and ocean surface for improving regional mesoscale model predictions. Preprints, *12th Conf. on Integrated Observing and Assimilation Systems for Atmosphere, Oceans, and Land Surface*, New Orleans, LA, Amer. Meteor. Soc., 13.5. [Available online at <http://ams.confex.com/ams/pdfpapers/131881.pdf>]
- Chen, F., and J. Dudhia, 2001: Coupling an advanced land-surface/hydrology model with the Penn State/NCAR MM5 modeling system. Part I: Model description and implementation. *Mon. Wea. Rev.*, **129**, 569-585.
- Davis, C. A., B. G. Brown, R. Bullock, and J. Halley-Gotway, 2009: The Method for Object-based Diagnostic Evaluation (MODE) applied to numerical forecasts from the 2005 NSSL/SPC Spring Program. *Wea. Forecasting*, **24**, 1252-1267.
- Derber, J. C., D. F. Parrish, and S. J. Lord, 1991: The new global operational analysis system at the National Meteorological Center. *Wea. Forecasting*, **6**, 538-547.
- Dudhia, J., 1989: Numerical study of convection observed during the winter monsoon experiment using a mesoscale two-dimensional model. *J. Atmos. Sci.*, **46**, 3077-3107.
- Ek, M. B., K. E. Mitchell, Y. Lin, E. Rogers, P. Grunmann, V. Koren, G. Gayno, and J. D. Tarpley, 2003: Implementation of Noah land surface model advances in the National Centers for Environmental Prediction operational mesoscale Eta model. *J. Geophys. Res.*, **108** (D22), 8851, doi:10.1029/2002JD003296.
- Gutman, G. and A. Ignatov, 1998: Derivation of green vegetation fraction from NOAA/AVHRR for use in numerical weather prediction models. *Int. J. Remote Sensing*, **19**, 1533-1543.
- Haines, S. L., G. J. Jedlovec, and S. M. Lazarus, 2007: A MODIS sea surface temperature composite for regional applications. *IEEE Trans. Geosci. Remote Sens.*, **45**, 2919-2927.
- Hong, S.-Y., and J.-O. J. Lim, 2006: The WRF single-moment 6-class microphysics scheme (WSM6). *J. Korean Meteor. Soc.*, **42**, 129-151.

- Janjić, Z. I., 1990: The step-mountain coordinate: Physical package. *Mon. Wea. Rev.*, **118**, 1429–1443.
- Janjić, Z. I., 1996: The surface layer in the NCEP Eta Model. Preprints, *Eleventh Conference on Numerical Weather Prediction*, Norfolk, VA, Amer. Meteor. Soc., 354–355.
- Janjić, Z. I., 2002: Nonsingular Implementation of the Mellor–Yamada Level 2.5 Scheme in the NCEP Meso model, NCEP Office Note, No. 437, 61 pp.
- Kumar, S. V., and Coauthors, 2006: Land Information System – An Interoperable Framework for High Resolution Land Surface Modeling. *Environmental Modeling & Software*, **21** (10), 1402–1415, doi:10.1016/j.envsoft.2005.07.004.
- Kumar, S. V., C. D. Peters-Lidard, J. L. Eastman, and W.-K. Tao, 2007: An integrated high-resolution hydrometeorological modeling testbed using LIS and WRF. *Environmental Modeling & Software*, **23** (2), 169–181, doi: 10.1016/j.envsoft.2007.05.012.
- LaCasse, K. M., M. E. Splitt, S. M. Lazarus, and W. M. Lapenta, 2008: The impact of high-resolution sea surface temperatures on the simulated nocturnal Florida marine boundary layer. *Mon. Wea. Rev.*, **136**, 1349–1372.
- Lin, Y., and K. E. Mitchell, 2005: The NCEP Stage II/IV hourly precipitation analyses: Development and applications. Preprints, *19th Conf. on Hydrology*, San Diego, CA, Amer. Meteor. Soc., 1.2. [Available online at <http://ams.confex.com/ams/pdfpapers/83847.pdf>]
- Lin, Y., K. E. Mitchell, E. Rogers, and G. J. DiMego, 2005: Using hourly and daily precipitation analyses to improve model water budget. Preprints, Ninth Symp. on Integrated Observing and Assimilation Systems for the Atmosphere, Oceans, and Land Surface, San Diego, CA, Amer. Meteor. Soc., 3.3. [Available online at <http://ams.confex.com/ams/pdfpapers/84484.pdf>]
- Miller, D. A. and R. A. White, 1998: A Conterminous United States multi-layer soil characteristics data set for regional climate and hydrology modeling. *Earth Interactions*, 2. [Available on-line at <http://EarthInteractions.org>].
- Mlawer, E. J., S. J. Taubman, P. D. Brown, M. J. Iacono, and S. A. Clough, 1997: Radiative transfer for inhomogeneous atmosphere: RRTM, a validated correlated-k model for the long-wave. *J. Geophys. Res.*, **102** (D14), 16663–16682.
- Robinson, D. A. and G. Kukla, 1985: Maximum surface albedo of seasonally snow covered lands in the Northern Hemisphere. *J. Climate Appl. Meteor.*, **24**, 402–411.
- Schaefer, G. L., M. H. Cosh, and T. J. Jackson, 2007: The USDA Natural Resources Conservation Service Soil Climate Analysis Network (SCAN). *J. Atmos. Oceanic Technol.*, **24**, 2073–2077.
- Skamarock, W. C., J. B. Klemp, J. Dudhia, D. O. Gill, D. M. Barker, M. G. Duda, X.-Y. Huang, W. Wang and J. G. Powers, 2008: A Description of the Advanced Research WRF Version 3, NCAR Technical Note, NCAR/TN–475+STR, 123 pp. [Available on-line at: [http://www.mmm.ucar.edu/wrf/users/docs/arw\\_v3.pdf](http://www.mmm.ucar.edu/wrf/users/docs/arw_v3.pdf)]
- Skamarock, W. C., and M. L. Weisman, 2009: The impact of positive-definite moisture transport on NWP precipitation forecasts. *Mon. Wea. Rev.*, **137**, 488–494..
- Smagorinsky J., S. Manabe, and J. L. Holloway Jr., 1965: Numerical results from a nine-level general circulation model of the atmosphere. *Mon. Wea. Rev.*, **93**, 727–768.

**Table 1.** A list of the LIS land surface fields and corresponding names in the WPS “METGRID.TBL” file, as used to initialize the LISMOD experimental WRF model runs.

| Land Surface Field          | Name in WPS “METGRID.TBL” |
|-----------------------------|---------------------------|
| Canopy Water*               | CANWAT                    |
| 0-10 cm Soil Moisture       | SM000010                  |
| 10-40 cm Soil Moisture      | SM010040                  |
| 40-100 cm Soil Moisture     | SM040100                  |
| 100-200 cm Soil Moisture    | SM100200                  |
| 0-10 cm Soil Temperature    | SM000010                  |
| 10-40 cm Soil Temperature   | SM010040                  |
| 40-100 cm Soil Temperature  | SM040100                  |
| 100-200 cm Soil Temperature | SM100200                  |
| Skin Temperature            | SKINTEMP                  |
| Snow Water Equivalent       | SNOW                      |

\*Canopy water is initialized to “0” in the default WRF source code.



0-10 cm Soil Moist Diff (LISMOD - CNTL) valid 080610/0300V000

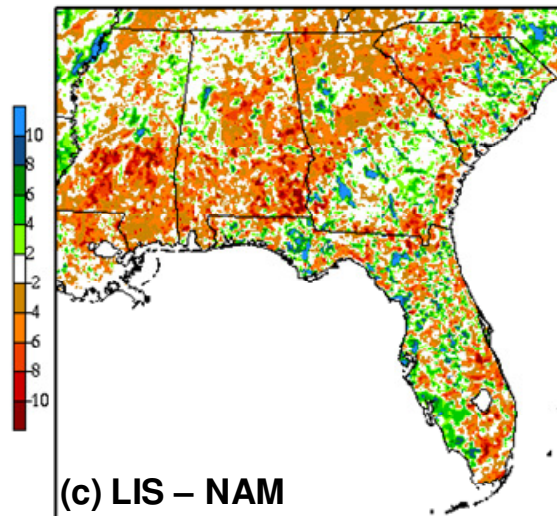


Figure 1. Comparison between WRF-initialized 0–10 cm volumetric soil moisture for the (a) Control (NAM model), (b) LISMOD (LIS spin-up), and (c) difference field (LISMOD – Control) valid at 0300 UTC 10 June 2008.

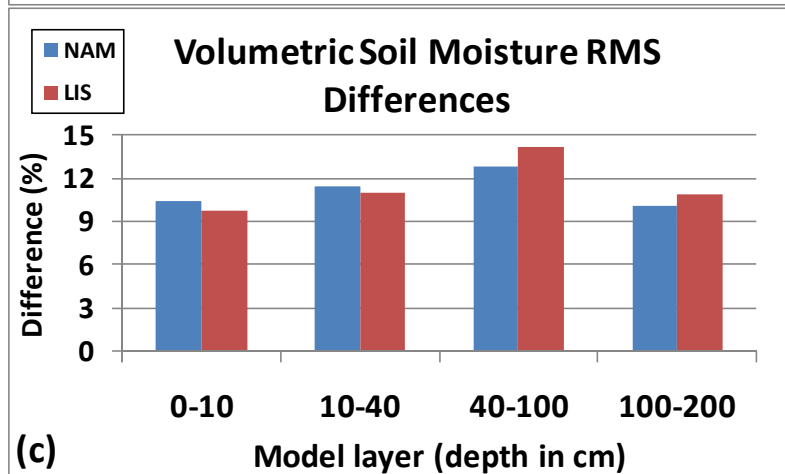
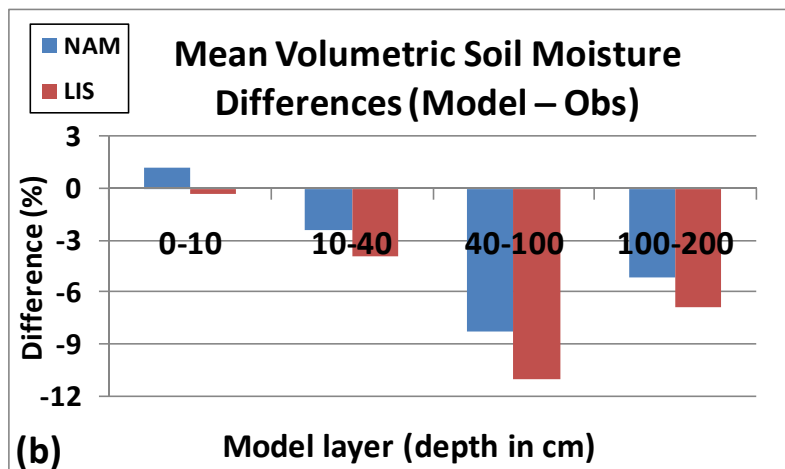
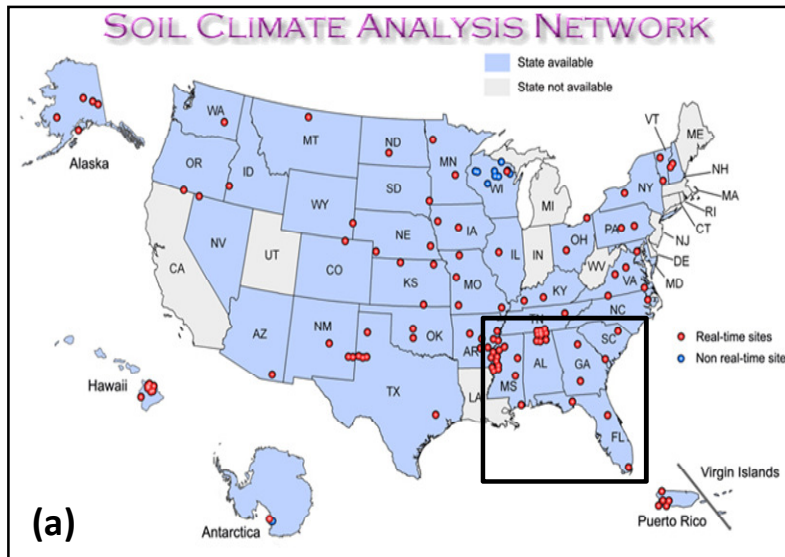


Figure 2. Validation of the NCEP/NAM (CON) and LIS volumetric soil moisture (%) against the Soil Climate Analysis Network (SCAN) observations at the model initialization hour, depicting (a) Bias or mean difference, and (b) Root-mean square (RMS) difference.

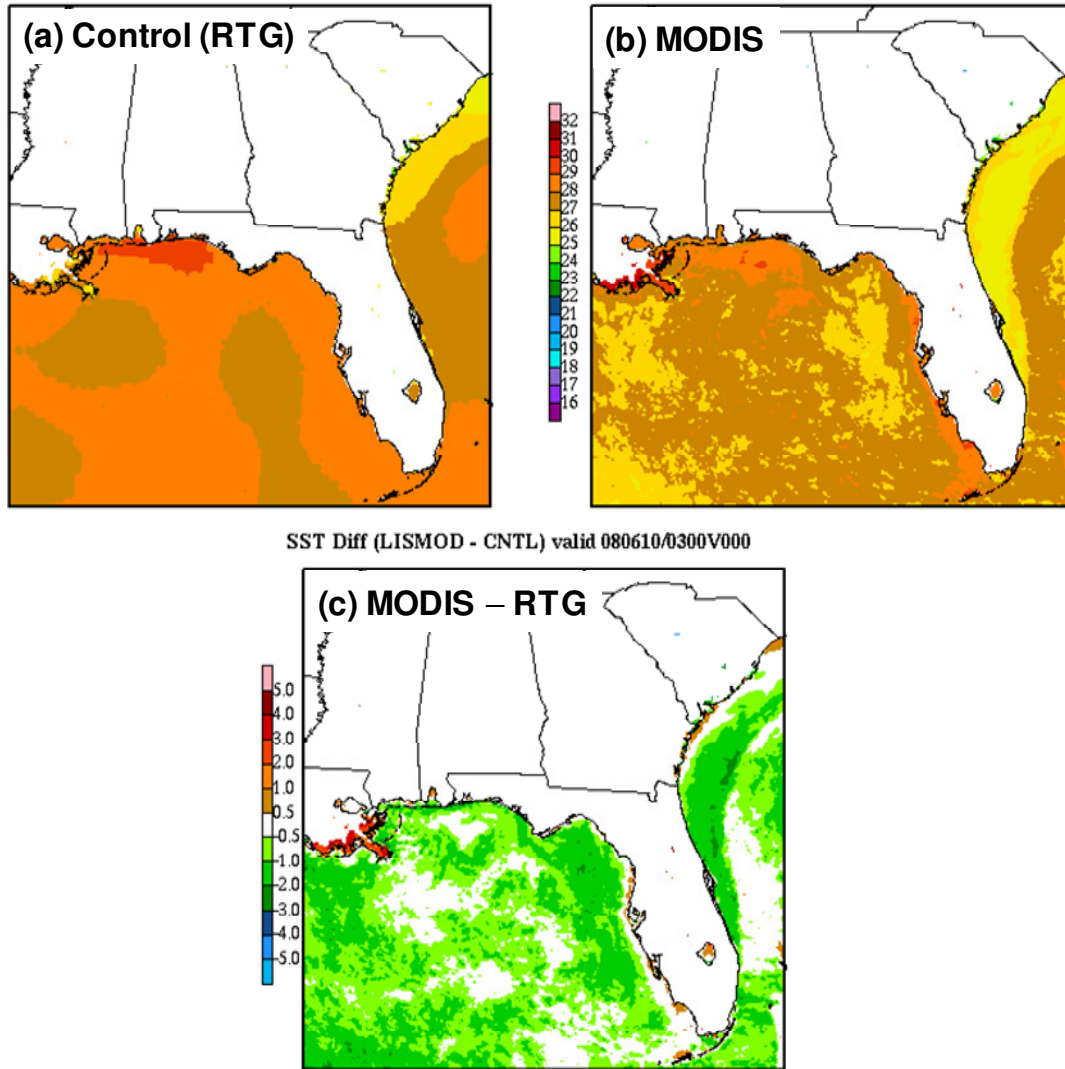
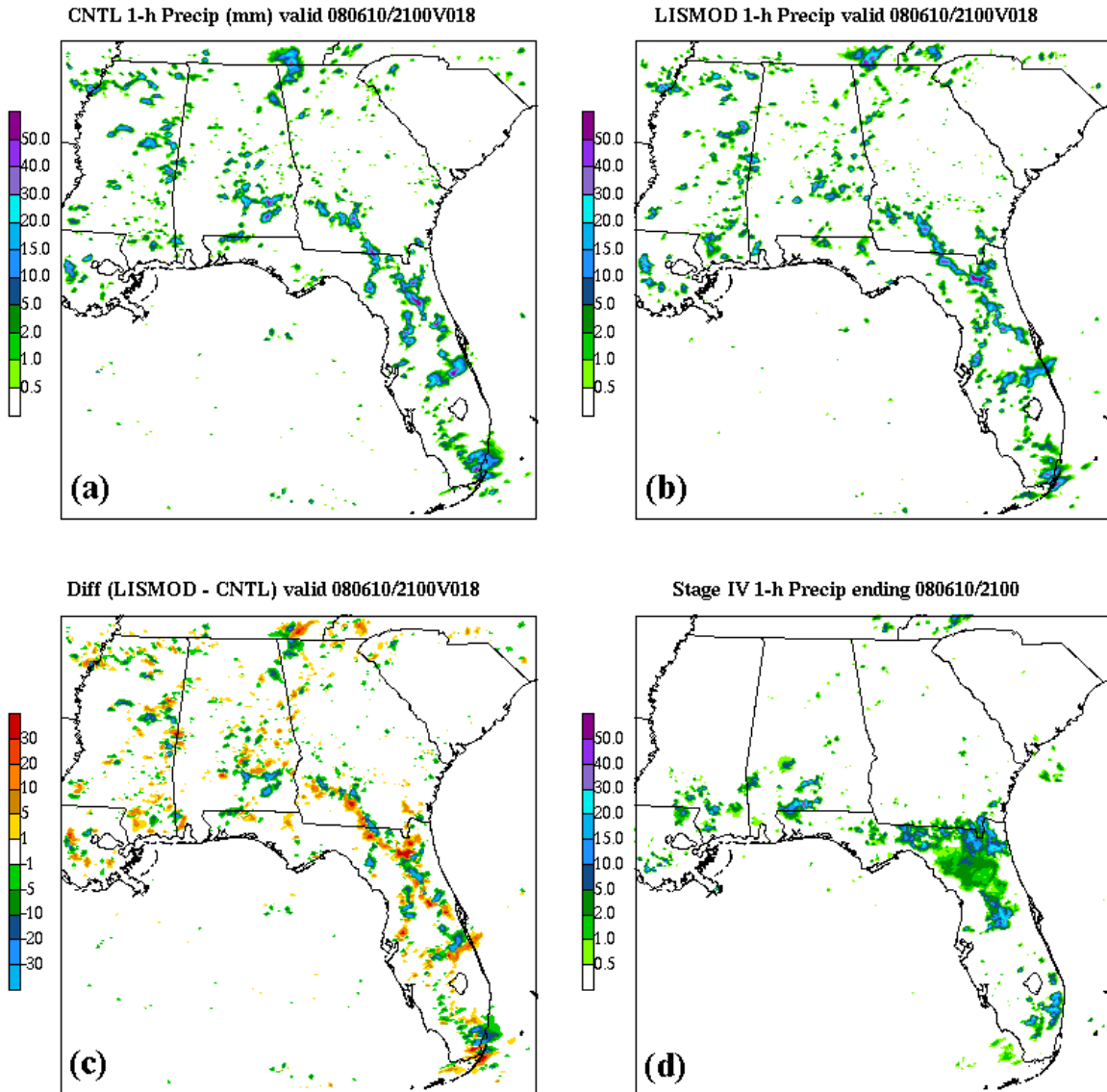


Figure 3. Comparison between WRF static SSTs for the (a) Control (NAM model / RTG product), (b) LISMOD (SPoRT MODIS data), and (c) difference field (LISMOD – Control), valid for the model run initialized at 0300 UTC 10 June 2008.



**Figure 4.** Comparison of accumulated precipitation (mm) for the 1-h period ending 2100 UTC 10 June 2008 for the (a) Control run, (b) LISMOD run, (c) difference between LISMOD and Control, and (d) Stage IV precipitation. Traditional grid point verification methods yield a Heidke Skill Score of 0 for the Control run and 0.015 for the LISMOD run over this time interval.

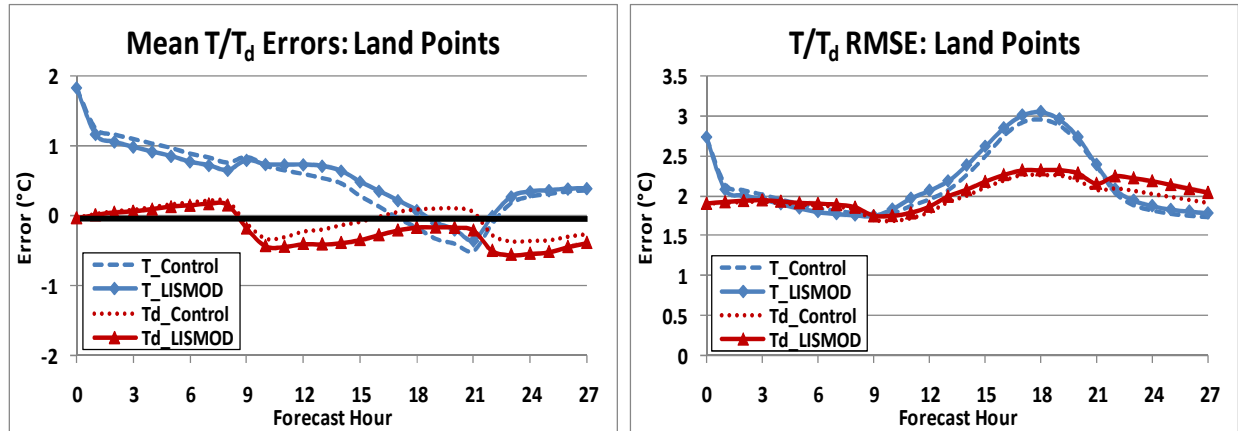


Figure 5. Comparison of 2-m temperature and dew point temperature model errors (°C) for 81 Control and LISMOD forecasts from June–August 2008 at approximately 500 surface observation locations. Plots shown are (a) mean error (bias), and (b) Root Mean Square Error (RMSE).

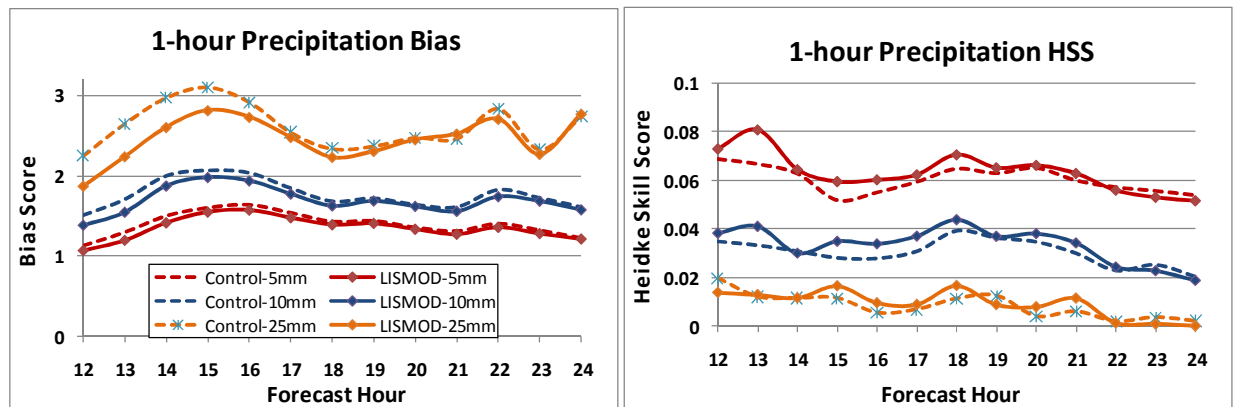
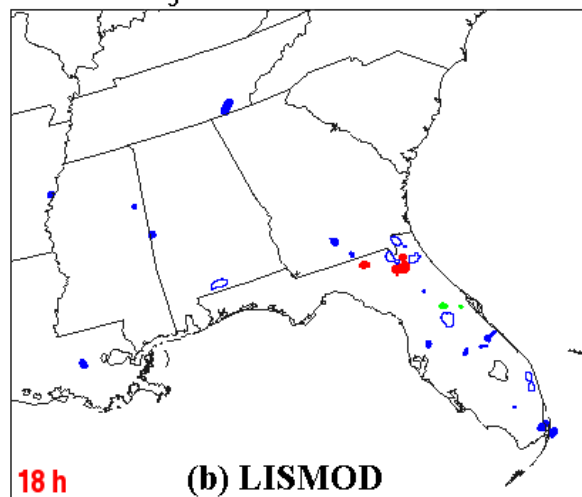
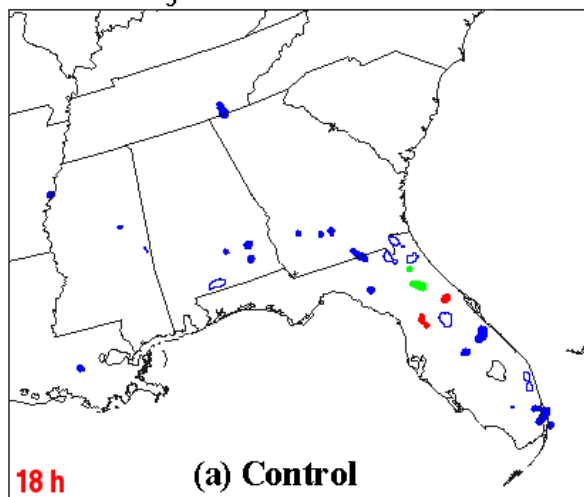


Figure 6. Traditional verification metrics of 1-h accumulated precipitation during the peak convective hours of 1500 UTC to 0300 UTC (forecast hours 12–24) for all 81 forecasts in the study period (June to August 2008). Plots shown are (a) Bias, and (b) Heidke Skill Score (HSS), according to the legend provided.

Table 2. MODE Fuzzy engine weights applied to object attributes to compute “total interest” field.

| Object Attribute             | Weight |
|------------------------------|--------|
| Centroid distance            | 20%    |
| Minimum boundary distance    | 40%    |
| Orientation angle difference | 10%    |
| Ratio of object areas        | 10%    |
| Intersection area ratio      | 20%    |

Forecast Objects with Observation Outlines      Forecast Objects with Observation Outlines



Observation Objects with Forecast Outlines      Observation Objects with Forecast Outlines

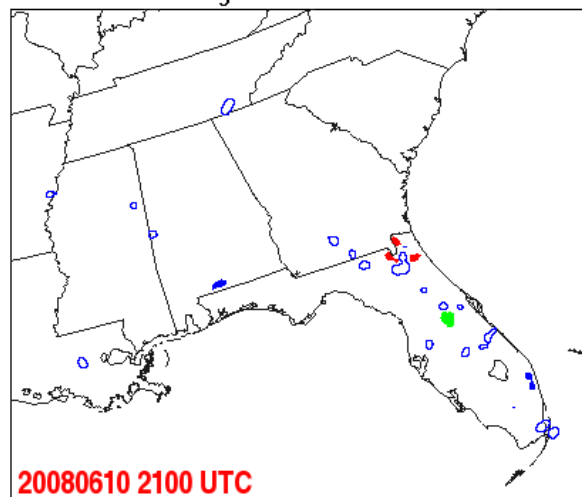
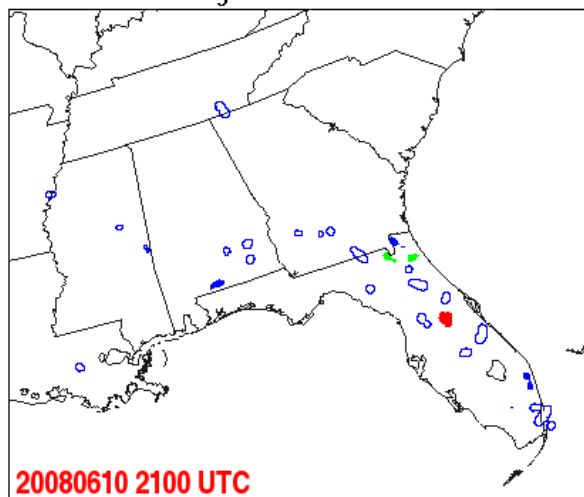


Figure 7. Comparison of 18-h forecast and Stage IV (observed)  $\geq 10$ -mm accumulated precipitation objects for the 1-h period ending 2100 UTC 10 June 2008 for the (a) Control run, and (b) LISMOD run. Solid blue shading indicates a false alarm in the forecast field or a forecast miss in the observed field. All other solid colors represent matched forecast or observed objects. Outlined blue areas denote the corresponding observed (forecast) objects in the field of forecast (observed) objects.

Table 3. Comparison between the total matched and unmatched areas (in number of grid points) of the 10-mm (1 h)<sup>-1</sup> precipitation objects in the Control and LISMOD runs initialized at 0300 UTC 10 June 2008. The valid times span from 1500 UTC 10 June to 0300 UTC 11 June. The better matched/unmatched numbers are in *bold-italics* font.

|               | Control      |                | LISMOD       |                |
|---------------|--------------|----------------|--------------|----------------|
| Forecast Hour | Matched Area | Unmatched Area | Matched Area | Unmatched Area |
| 12            | 0            | 115            | 0            | 115            |
| 13            | 0            | 93             | 0            | <b>64</b>      |
| 14            | 0            | 222            | 0            | <b>108</b>     |
| 15            | 0            | 492            | 0            | <b>474</b>     |
| 16            | 0            | 802            | <b>232</b>   | <b>587</b>     |
| 17            | 388          | <b>544</b>     | <b>606</b>   | 653            |
| 18            | 419          | 1039           | <b>470</b>   | <b>711</b>     |
| 19            | 108          | 1122           | <b>186</b>   | <b>916</b>     |
| 20            | <b>318</b>   | 680            | 271          | <b>674</b>     |
| 21            | <b>394</b>   | 301            | 382          | 646            |
| 22            | 0            | 596            | <b>110</b>   | <b>424</b>     |
| 23            | 28           | 632            | <b>30</b>    | <b>501</b>     |
| 24            | 0            | <b>328</b>     | 0            | 417            |

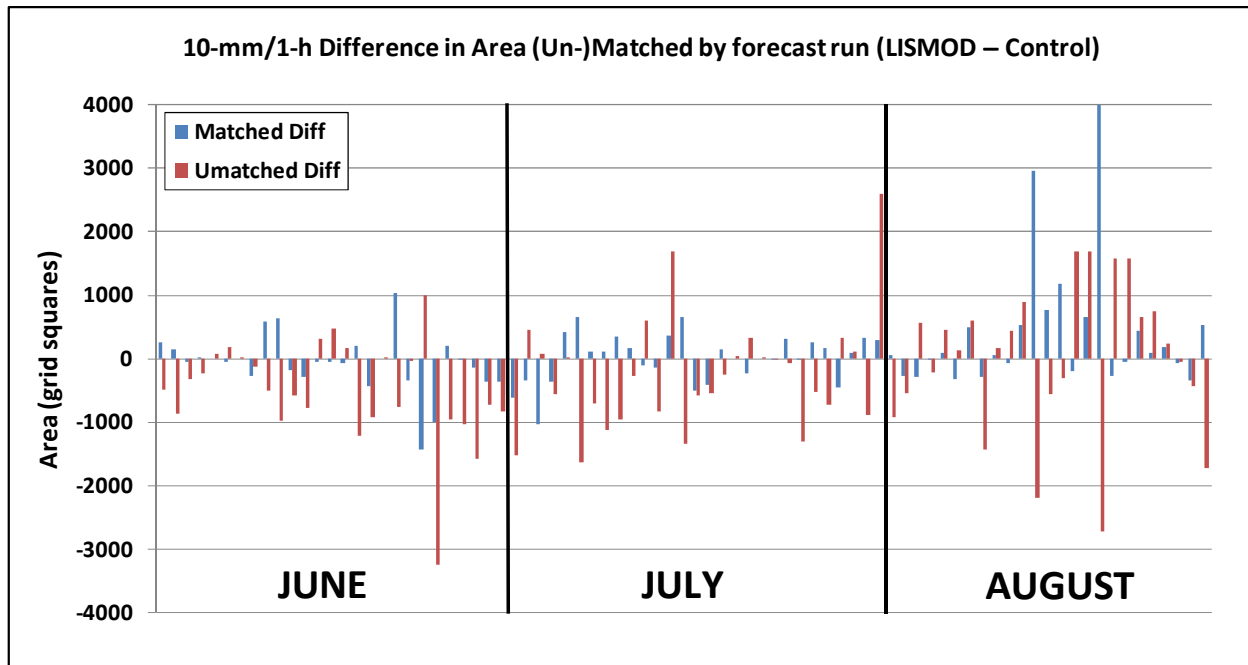


Figure 8. Difference in total matched and unmatched 10 mm per hour accumulated precipitation object areas during the peak convective hours (1500 UTC to 0300 UTC) for each individual forecast from June to August 2008. Blue bars indicate the difference in matched area while red bars indicate the difference in unmatched area.

| <b>Table 4. Mean matched and unmatched 1-h precipitation object areas for the Control and LISMOD per forecast run, and the percent improvement in LISMOD over the Control as a function of accumulated forecast interval. All 1-h forecasts during the peak convective hours are combined for each forecast run (12–24 h, corresponding to the 1500–0300 UTC window). Differences / % Changes in bold font indicate statistical significance at the 99<sup>th</sup> percentile while italics font indicates significance at the 90<sup>th</sup> percentile.</b> |         |        |                                  |              |
|---|---------|--------|----------------------------------|--------------|
| Quantity<br>(mean # grid points<br>per model run)   | Control | LISMOD | Difference<br>(LISMOD – Control) | % Change     |
| 5-mm Matched  | 11 911  | 12 045 | 134                              | 1.1%         |
| 5-mm Unmatched  | 17 750  | 17 175 | <b>-575</b>                      | <b>-3.2%</b> |
| 10-mm Matched   | 2 456   | 2 562  | <i>106</i>                       | <i>4.3%</i>  |
| 10-mm Unmatched   | 6 798   | 6 538  | <b>-260</b>                      | <b>3.8%</b>  |
| 25-mm Matched   | 60      | 60     | 0                                | 0%           |
| 25-mm Unmatched   | 549     | 505    | <b>-44</b>                       | <b>-8.0%</b> |

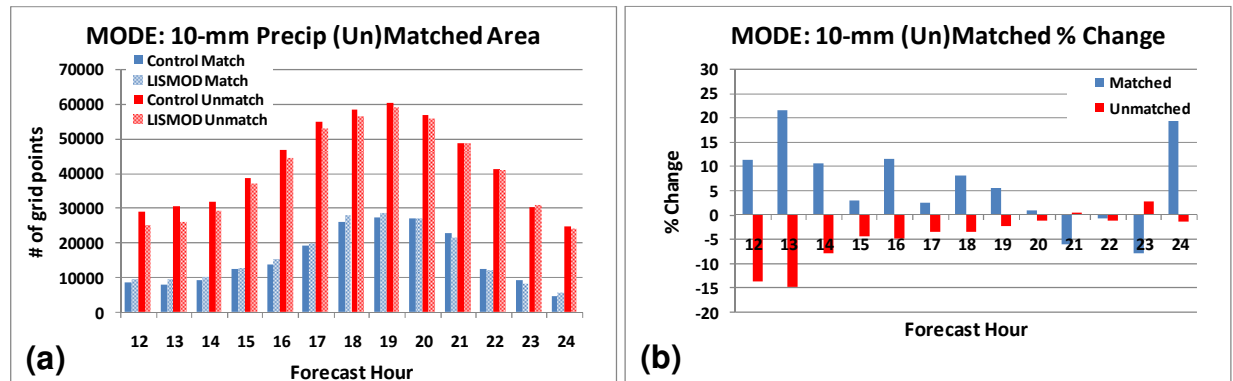


Figure 9. Comparison between the total matched and unmatched object areas from all 81 forecast cycles for 1-h accumulated precipitation  $\geq 10$  mm during the forecast hours centered on the diurnal peak convective activity (12–24 hours, valid 1500 UTC to 0300 UTC). (a) Total matched object area (blue bars) and unmatched object area (red bars) for the Control (solid bars) and LISMOD (hatched bars), and (b) LISMOD percentage change from the Control matched/unmatched object area.

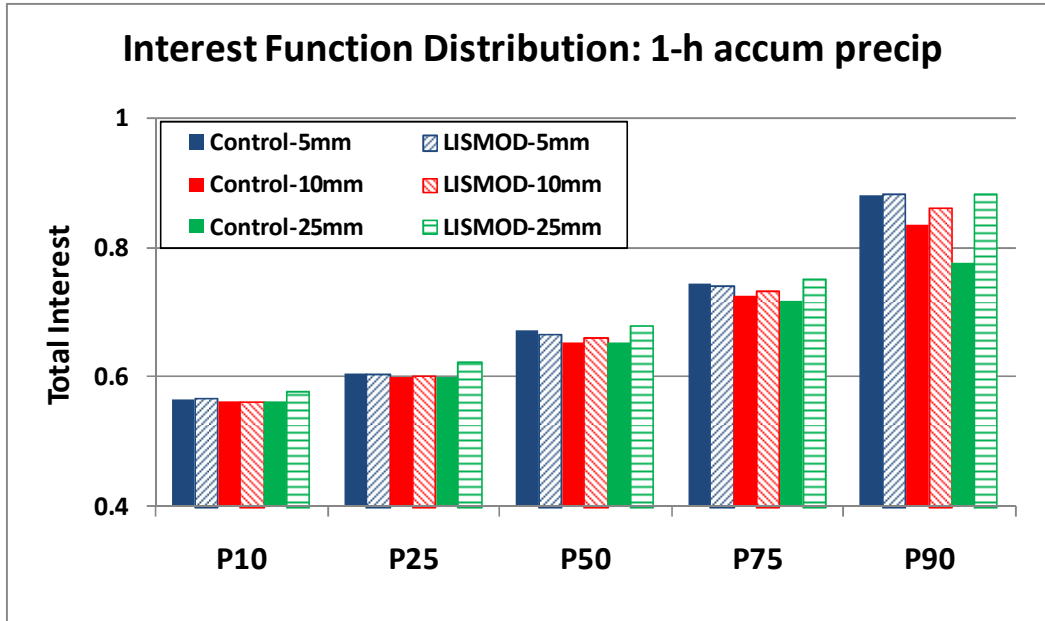


Figure 10. Distribution of the total interest function for all 81 Control and LISMOD forecast/observed 1-h accumulated precipitation object pairs during the peak convective hours of 1500 to 0300 UTC. The plot depicts the Control and LISMOD values within their respective interest function distributions at the 10th, 25th, 50th, 75th, and 90th percentiles for 5-mm, 10-mm, and 25-mm accumulated precipitation thresholds, according to the scale provided. The interest function sample sizes are provided in Table 5.

| Table 5. The number of 1-h accumulated precipitation object pairs at various thresholds composing the interest function distributions plotted in Figure 10. |      |       |       |
|---|------|-------|-------|
| Precipitation threshold   |      |       |       |
| WRF Experiment  | 5 mm | 10 mm | 25 mm |
| Control   | 8934 | 2479  | 74    |
| LISMOD  | 9077 | 2445  | 69    |